

Ultrasound-modulated optical microscopy

Sri-Rajasekhar Kothapalli

Lihong V. Wang

Washington University at St. Louis
Department of Biomedical Engineering
Optical Imaging Laboratory
St. Louis, Missouri 63130

Abstract. We demonstrate that microscopic imaging is feasible in ultrasound-modulated optical tomography (UOT) of soft biological tissues, using a high-frequency focused ultrasound transducer with a 75-MHz central frequency. Our experiments in tissue mimicking phantoms show that at an imaging depth of about 2 mm, an axial resolution better than $30\ \mu\text{m}$ can be achieved, whereas the lateral resolution is $38\ \mu\text{m}$. A long-cavity scanning confocal Fabry-Perot interferometer (CFPI) is used for real-time detection of multiply scattered light modulated by high-frequency ultrasound pulses propagating in an optically scattering medium. We also compare the performances of various high-frequency focused ultrasound transducers with central frequencies of 15 MHz, 30 MHz, 50 MHz, and 75 MHz. The comparison is based on two-dimensional (2-D) images of optically absorbing objects positioned at a few millimeters depth below the surface of both optically scattering phantoms and soft biological tissue samples. Our experimental results show that modulation depth and image contrast decrease with an increase in ultrasound frequency. In addition, we use analytical calculations to show that modulation depth decreases with increasing ultrasound frequency.

© 2008 Society of Photo-Optical Instrumentation Engineers. [DOI: 10.1117/1.2983671]

Keywords: ultrasound-modulated optical tomography (UOT); ultrasound; multiply scattered light; confocal Fabry-Perot interferometer (CFPI); microscopy.

Paper 08118R received Apr. 8, 2008; revised manuscript received Jun. 24, 2008; accepted for publication Jul. 8, 2008; published online Oct. 9, 2008.

1 Introduction

In recent years, optical imaging modalities have become capable of providing functional, structural, and molecular information about tissue based on various optical contrast mechanisms. In addition, the technical advantages, such as nonionizing radiation, ease of operation, low cost, and high sensitivity have advanced these technologies to biomedical applications.¹⁻⁵ Many *in vivo* optical microscopy techniques offer micron-scale resolution at shallow (a few hundred μm) imaging depths in the skin. They are mainly based on the ballistic component of back-reflected light for imaging while rejecting multiply scattered light.

Ultrasound-modulated optical tomography (UOT) has been proposed to achieve high-resolution tomographic imaging using multiply scattered light.^{6,7} In this hybrid imaging modality, a focused ultrasonic wave tags diffuse coherent light in scattering biological tissue. The physical mechanism of the modulation can be attributed to ultrasound-induced displacements of optical scatterers and ultrasound-induced changes in the optical index of refraction.⁸⁻¹² The volume occupied by both the ultrasound and the light beam can be approximated as the source of the modulated light. Consequently, the measured modulation signal is much more sensitive to the optical properties of tissue within the ultrasound beam than the measured nonmodulated light intensity.¹³ Thus, this imaging mo-

dality combines ultrasonic resolution and optical contrast. In addition, mechanical contrast of soft biological tissue can also be imaged by time-gating the modulated light.¹⁴ Various detection schemes have been proposed to detect ultrasound-modulated light.¹⁵⁻²⁴ A computed tomography method for UOT has also been proposed.²⁵ At present, detection schemes based on the Fabry-Perot interferometers²³ or photorefractive crystals²⁴ are the most suitable choices for fast parallel speckle detection.

In this article, we study the feasibility of microscopic imaging using a high-frequency ultrasound transducer with a 75-MHz central frequency. Our experiments in an optically scattering medium and in chicken breast tissue show that lateral resolution of $38\ \mu\text{m}$ and axial resolution better than $30\ \mu\text{m}$ can be achieved at imaging depths of about 2 mm. We use a long-cavity scanning confocal Fabry-Perot interferometer (CFPI) for real-time detection of multiply scattered light modulated by the high-frequency ultrasound pulses propagating in biological tissue. The CFPI has a greater etendue than most CCD cameras and provides parallel speckle processing. In addition, the CFPI can detect the propagation of high-frequency ultrasound pulses in real time while tolerating speckle decorrelation. Compared to the other approaches for the detection of UOT signals, the CFPI is especially efficient at selectively transmitting signals modulated at high ultrasound frequencies. As in our recent proceedings article,²⁶ we compare the performances of various high-frequency focused

Address all correspondence to Lihong V. Wang, Washington Univ. at St. Louis, Dept. of Biomedical Engineering, Optical Imaging Laboratory, St. Louis, MO 63130. E-mail: lhwang@biomed.wustl.edu

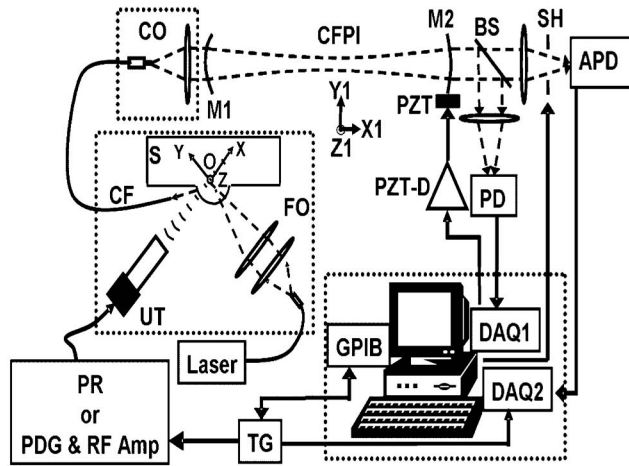


Fig. 1 Schematic of the experimental setup: APD, avalanche photodiode; BS, beamsplitter; CF, collecting fiber; CFPI, confocal Fabry-Perot interferometer; CO, coupling optics; DAQ, data acquisition board; FO, focusing optics; M1, M2, mirrors inside the cavity; PD, photodiode; PDG, pulse delay generator; PR, pulser-receiver; PZT, piezoelectric transducer; PZT-D, piezoelectric transducer driver; RF Amp, RF amplifier; S, sample; SH, shutter; TG, trigger generator; UT, ultrasonic transducer.

ultrasound transducers, with central frequencies of 15 MHz, 30 MHz, 50 MHz, and 75 MHz, used in our UOT experiments. Last, we study the effect of ultrasound frequency on the modulation depth, using UOT experiments and analytical calculations.

2 Experimental Methods

2.1 Experimental Setup

We used a CFPI, proposed for UOT by Sakadzic and Wang,²³ to detect in real time the multiply scattered light modulated by high-frequency ultrasound pulses propagating in an optically scattering medium. The details of the CFPI experimental setup (Fig. 1) used to detect the UOT signals have been described earlier.²³ Figure 1 shows the configuration of the sample S that is imaged, as well as the orthogonal configuration of the light illumination and ultrasound insonification of the sample S. Our study showed that this configuration minimized the contribution of the unmodulated light from the shallow regions to the background. In addition, it enhanced the interaction between the ultrasound and some quasi-ballistic light that still existed at small imaging depths (up to one optical transport mean free path). A circular tissue sample, 1 cm in thickness and 3 cm diameter, was gently pressed through a slit along the z axis to create a semicylindrical bump in radius of 1.5 to 3 mm. The orthogonal ultrasonic and optical beams were focused to the same spot below the sample surface. In the experiment, the laser light (Coherent, Verdi; 532-nm wavelength) was focused onto a spot $\sim 100 \mu\text{m}$ in diameter below the surface of an otherwise scattering-free sample. The optical power delivered to the sample was between 100 mW and 300 mW, depending on the type of sample and the center frequency of the transducer.

Although the CW power in this proof-of-principle experiment exceeded the ANSI safety limit for average power, the duration of the light exposure to the sample can be reduced to only a few μs for each cycle of ultrasound propagation through the region of interest, and therefore, the safety limit will not be exceeded in the end, even if the light is focused into a scattering medium.

Diffusely transmitted light was collected by a multimode optical fiber with a 600- μm core diameter (0.37 numerical aperture [NA] and 0.12 mm^2 sr etendue). As shown in Fig. 1, the detection fiber (CF) is placed as closely to the sample as possible without scratching the sample during the scanning procedure. The axes of propagation of the ultrasonic and optical beams are denoted by X and Y, respectively. The sample was mounted on a three-axis (X_1 , Y_1 , and Z_1) translational stage. The ultrasound transducer UT and the sample S were immersed in water for acoustic coupling, and thus the light focusing optics FO and the collecting fiber CF were also immersed in the same water tank. The collected light was coupled into the CFPI, using coupling optics CO, and was operated in transmission mode (50-cm cavity length, 0.1- mm^2 sr etendue, and ~ 20 finesse).

The filtered light sampled by the beam sampler (5:95) and detected by the photodiode PD (New Focus Model 2031) was used in a cavity alignment procedure. The cavity was first swept through one free spectral range to find the position of the central frequency of the unmodulated light. Then, CFPI mirror M2 was displaced by a calibrated amount so that the cavity was tuned to the frequency of one sideband of the ultrasound-modulated light (15 MHz, 30 MHz, 50 MHz, or 75 MHz greater than the laser light frequency). The filtered light transmitted by the beam sampler was detected by an avalanche photodiode (APD; Advanced Photonix), and the signal was sampled at 200 Ms/sec with a data acquisition board (GAGE, CS14200). A LabView computer program controlled the movement of the CFPI mirror and the other sequences of the control signals. A trigger generator (Stanford Research, DG535) triggered both the ultrasound pulse generation and the data acquisition from the APD. Since the resonant frequency of the CFPI cavity coincided with one sideband of the ultrasound-modulated light, the signal acquired by the APD during the ultrasound propagation through the sample represented the distribution of the ultrasound-modulated optical intensity along the ultrasonic axis and, therefore, yielded a one-dimensional (1-D) image (A-line) along the x direction. In each operational cycle, the resonant frequency of the CFPI was tuned first, and then data from 4000 ultrasound pulses were acquired in one second. Averaging over 10 to 50 cycles was usually necessary to obtain a satisfactory SNR for each 1-D image. Two-dimensional (2-D) images were obtained by scanning the sample along the z direction and acquiring each corresponding 1-D image.

In our experiments, we used four high-frequency ultrasound transducers with central frequencies of 15 MHz, 30 MHz, 50 MHz, and 75 MHz. As shown in Fig. 2(a), the 15-MHz transducer (Ultran, fused silica delay line, 4.7-mm lens diameter, 4.7-mm focal length, 15-MHz estimated bandwidth) was driven by a pulser (GE Panametrics, 5072PR). The transducers with central frequencies of 30 MHz, 50 MHz, and 75 MHz (GE Panametrics, 4.25- μs fused silica delay

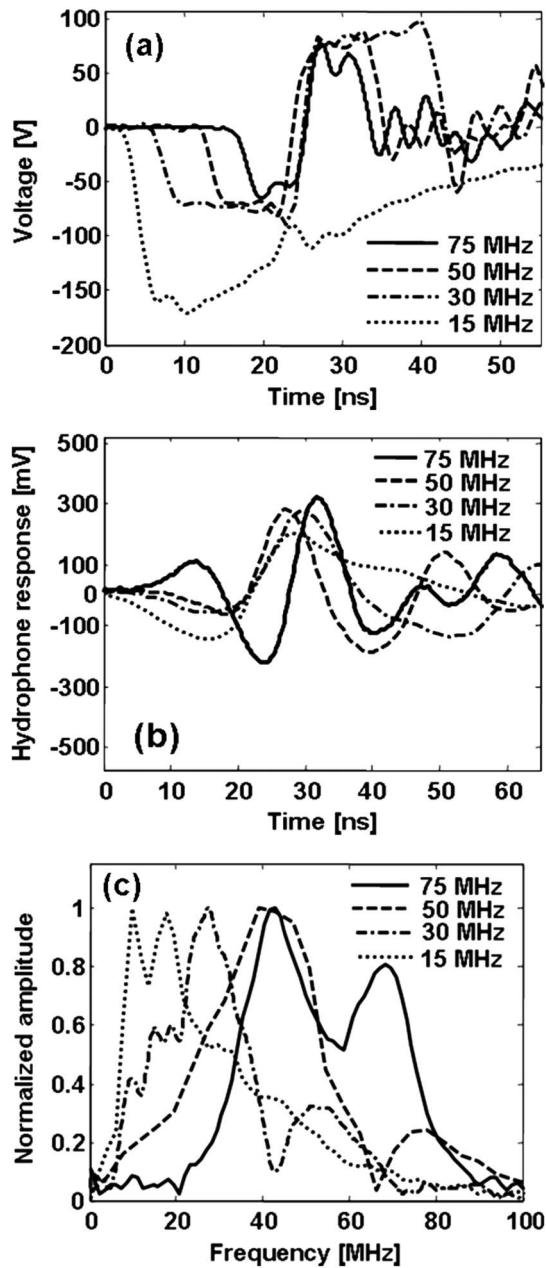


Fig. 2 (a) Driving pulses of all four ultrasound transducers. (b) Hydrophone responses of the transducers in response to respective driving pulses. (c) Frequency spectra of (b).

lines, 0.25-in element sizes, 5.5-mm focal lengths, 80% estimated fractional bandwidths for 30 and 50 MHz and 85% for the 75 MHz) were driven by the square bipolar pulses with periods of 34 ns, 20 ns, and 15 ns, respectively. These bipolar pulses are generated by the trigger generator (Stanford Research, DG535) and amplified with an amplifier (Amplifier Research, 75A250) and are shown in Fig. 2(a). Figure 2(b) shows the focal ultrasound pressure measured by the needle hydrophone (ONDA HNV-0200) for all four transducers. For all four transducers, the peak pressure was between 2 MPa and 4 MPa, within the ultrasound safety limit at these frequencies for tissues without well-defined gas bodies.²⁷ The

Fourier spectra of respective hydrophone responses are shown in Fig. 2(c).

2.2 Phantom Preparation

Since in ultrasound-modulated optical tomography (UOT), we primarily aim to image optical contrast of soft biological tissue, we need to prepare light absorbing or scattering objects that are transparent to ultrasound in our experiments with phantoms. Objects made from cutting 100- μm -thick latex sheets are transparent enough to ultrasound. We prepared several resolution targets using these latex sheets and dyed them with black ink. The tails of these resolution targets were then glued into the barrels of 31-gauge needles with an outside diameter of 254 μm . These resolution targets attached to the needle were then buried several mm below either chicken breast tissue or tissue-mimicking Intralipid phantoms. Since ultrasound waves are strongly reflected by the needle, it helped in aligning the resolution targets precisely at the ultrasound focal point. We used a pulser (GE Panametrics, 5072PR) in this alignment procedure. The optically scattering sample was prepared from 2% agar and 1% Intralipid (20% Liposyn II, Intravenous Fat Emulsion, Hospira, Inc.), with a 1-mm optical transport mean free path and with either a 3-mm or a 2-mm radius of curvature in the cylindrical bump. Resolution targets were placed in the center of the curvature of the prepared sample, i.e., 3 mm or 2 mm below the surface of the sample.

3 Results and Discussion

3.1 Lateral and Axial Resolution Measurements

To investigate the axial and lateral resolutions of various high-frequency ultrasound transducers with central frequencies of 15 MHz, 30 MHz, 50 MHz, and 75 MHz, we imaged light absorbing objects made from 100- μm -thick latex buried inside the chicken breast tissue. The target is 100 μm thick along the x axis (i.e., the axial direction, and also the ultrasound propagation direction), 100 μm wide along the y axis (the light propagation direction), and about 1 mm in length along the z axis (the lateral direction). A photograph of this absorbing object is shown in Fig. 3(a). Figure 3(b) shows typical A-lines for all four transducers where a 2-mm shift was added successively to the origin of A-lines of 30 MHz, 50 MHz, and 75 MHz to display all four curves. These A-lines represent the temporal dependence of the ultrasound-modulated light intensity during ultrasound-pulse propagation through the sample. For each A-line, the time of propagation is multiplied by 1500 ms^{-1} , the approximate speed of sound in the sample, to be converted to distance along the x axis, where the origin of each A-line corresponds to the trigger for the signal acquisition from the APD. Two-dimensional (B-scan) images using all four transducers were obtained by scanning the sample along the z direction. Figures 3(c)–3(f) show 2-D images of Fig. 3(a) obtained with 15-MHz, 30-MHz, 50-MHz, and 75-MHz central frequency transducers at approximate depths of 2.5 mm, 2 mm, 1.5 mm, and 1.2 mm below the chicken breast tissue, respectively. All these 2-D images were cropped to some extent (a few hundred μm at the beginning and at the end of each image that has gray level below 0.2) along the axial direction to present clear

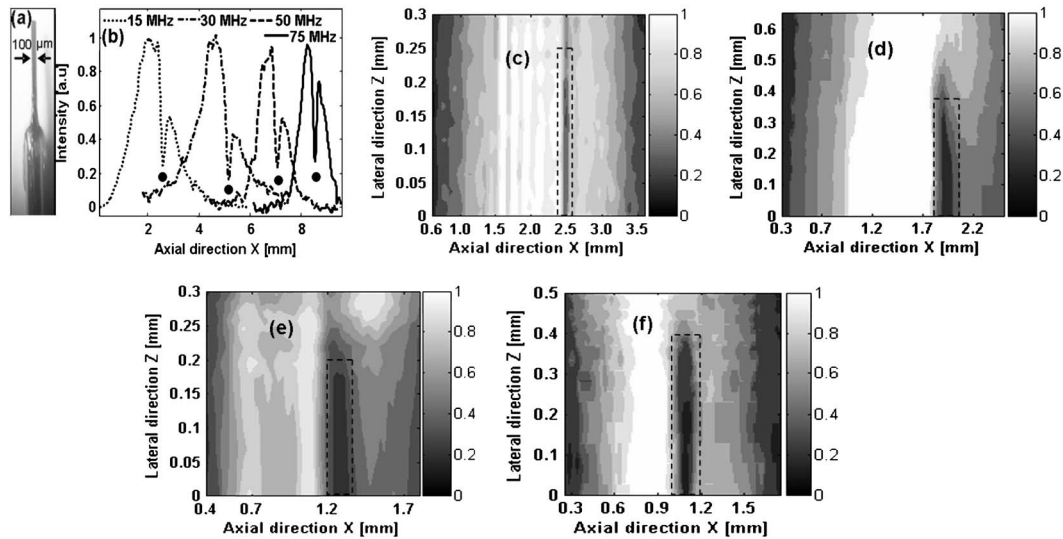


Fig. 3 Imaging 100- μm -wide light absorbing object using all four transducers. (a) Photograph of the object. (b) A-lines for different high-frequency transducers that represent temporal dependence of ultrasound-modulated light intensity during the propagation of the ultrasound pulse through the chicken breast tissue sample. A dot placed below each curve in the figure represents the position of the object along the ultrasound propagation direction. B-scan UOT images of (a) inside the chicken breast tissue sample obtained with (c) the 15-MHz transducer below the depth of 2.5 mm, (d) the 30-MHz transducer below the depth of 2 mm, (e) the 50-MHz central frequency transducer below the depth of 1.5 mm, and (f) the 75-MHz transducer at about 1 mm depth. In all B-scan images, the object is enclosed in a dashed rectangle.

images. Therefore for all four transducers, the approximate depth of the object (shown as a dot below the position of the object in each A-line) was estimated from the origin of respective A-lines shown in Fig. 3(b).

In pure ultrasound imaging, the higher the ultrasound frequency, the better the resolution of the image is. However, the attenuation of ultrasound energy also increases with the frequency, and this limits the penetration depth of the ultrasound pulse. The same can be inferred from our UOT experimental results, shown in Fig. 3. For all four transducers, the approximate extent of modulated light along the axial direction was estimated from respective A-lines shown in Fig. 3(b). The extent of modulated light for 15-MHz, 30-MHz, 50-MHz, and 75-MHz central frequency transducers is about 3 mm, 2.5 mm, 2.3 mm, and 1.8 mm respectively.

In all our experiments, we also noticed that the modulated light intensity was measurable almost immediately after the ultrasound pulse entered the sample. Although visible light has been strongly scattered beyond the 1-mm light transport mean free path, focusing the light beam still helps to increase the amount of light in the ultrasound focal zone. But light focusing has very little influence on resolution in our experiment, as the resolution in UOT is predominantly determined by the ultrasound parameters.

In pure ultrasound imaging, the lateral resolution ($\lambda F/D$) is related to the width of the ultrasound beam at the focus. The axial resolution depends on the length of the ultrasound pulse and is usually FWHM of the ultrasound pulse length. Here λ is the wavelength of the ultrasound, F is the focal length of the transducer, and D is the element size. Table 1 shows our experimental measurements of focal width and focal length in water for all four transducers, when driven by the respective driving pulses, as shown in Fig. 2(a). We estimated the lateral and axial resolutions of UOT images, shown in Figs.

3(c)–3(f), obtained with the four high-frequency transducers with central frequencies 15 MHz, 30 MHz, 50 MHz, and 75 MHz, respectively, based on the respective edge spread functions of the absorbing object. Figures 4(a) and 4(b) show typical axial and lateral edge spread functions of the absorbing object, respectively, obtained with all four transducers, 15 MHz, 30 MHz, 50 MHz, and 75 MHz. We define lateral and axial resolutions as the one-way distance between the 25% and 75% points (as marked by dashed arrows in the figures) of the respective edge spread functions. In Table 1, we also report the mean (with a standard deviation of about two to three microns) values of the lateral and axial resolutions for all four transducers, calculated from several respective measurements of lateral and axial edge spread functions of the absorbing object. For the transducer with 15-MHz

Table 1 Summary of ultrasound source parameters and measured axial and lateral resolutions and imaging depth in UOT experiments for all four transducers.

Frequency	Band width	Focal width	Focal depth	Resolution using edge spread function		Imaging depth
				Axial	Lateral	
15 MHz	100%	90 μm	4.7 mm	74 μm	140 μm	3.0 mm
30 MHz	80%	55 μm	5.5 mm	60 μm	70 μm	2.5 mm
50 MHz	80%	33 μm	5.5 mm	48 μm	55 μm	2.3 mm
75 MHz	85%	25 μm	3.0 mm	31 μm	38 μm	1.8 mm

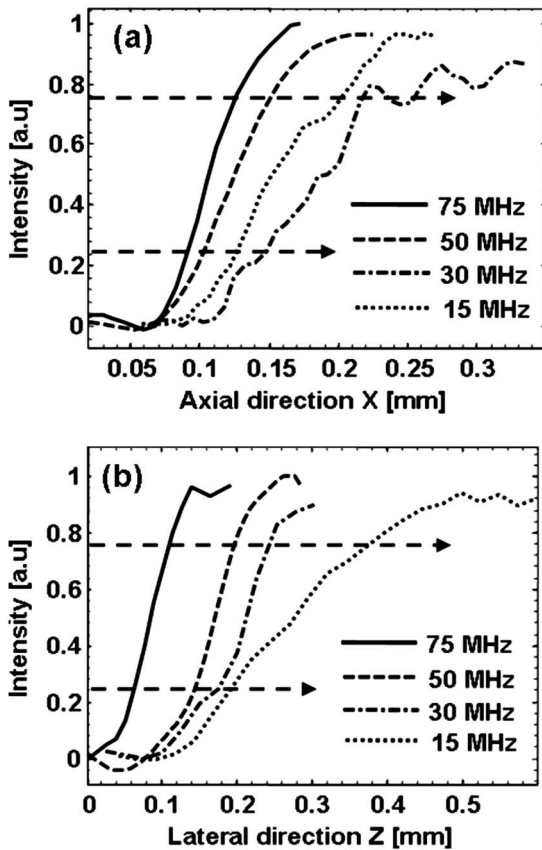


Fig. 4 Measurement of the axial and lateral resolutions of the UOT images shown in Fig. 3, obtained with all four high-frequency ultrasound transducers. (a) Axial edge spread functions, and (b) lateral edge spread functions of UOT signals for respective high-frequency ultrasound transducers.

central frequency, a lateral resolution of $140\ \mu\text{m}$ and an axial resolution of $74\ \mu\text{m}$ in a depth range of 3 mm inside the chicken breast tissue are measured. Similarly 30-MHz, 50-MHz, and 75-MHz central frequency transducers provided axial resolutions of $60\ \mu\text{m}$ (in a depth range of 2.5 mm), $48\ \mu\text{m}$ (in a depth range of 2.3 mm), and $31\ \mu\text{m}$ (in a depth range of 1.8 mm), respectively, inside the chicken breast tissue. Their lateral resolutions were $70\ \mu\text{m}$, $55\ \mu\text{m}$, and $38\ \mu\text{m}$, respectively.

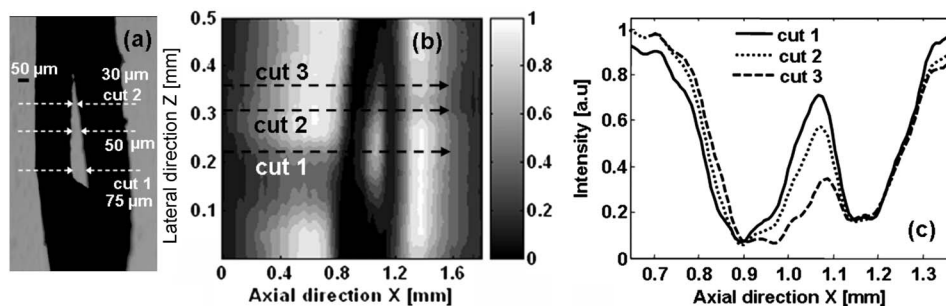


Fig. 5 Imaging of high-resolution axial target located 2.0 mm inside the tissue-mimicking phantom using 75-MHz transducer. (a) Photograph of axial resolution target marked with two different sizes of gap; cut 1= $75\ \mu\text{m}$ and cut 2= $30\ \mu\text{m}$. (b) B-scan UOT image of (a) marked with the respective cuts and cut 3= $15\ \mu\text{m}$. (c) Three 1-D axial profiles, from the intensity data in (b), corresponding to three different cuts shown in (b).

To further investigate the potential of microscopic imaging in UOT, we used the 75-MHz transducer to image an axial resolution target, as shown in Fig. 5(a), that was buried about 2.0 mm below the optical scattering sample (made of agar gel and Intralipid) of 1-mm optical transport mean free path. The target has dimensions of about $400\ \mu\text{m}$ (including gap) along the x axis, $100\ \mu\text{m}$ along the y axis, and about $500\ \mu\text{m}$ along the z axis. In Fig. 5(b), we present the corresponding B-scan UOT image of Fig. 5(a). From Fig. 5(b), we estimate that, cut 1 at lateral position $Z=0.21\ \text{mm}$ has a gap width of $75\ \mu\text{m}$, cut 2 at lateral position $Z=0.32\ \text{mm}$ has a gap width of $30\ \mu\text{m}$, and cut 3 at lateral position $Z=0.36\ \text{mm}$ has a gap width of $15\ \mu\text{m}$. Figure 5(c) represents the 1-D axial intensity profiles along the x axis for the three cuts, obtained from the image in Fig. 5(b). This graph shows that axial widths of $75\ \mu\text{m}$, $30\ \mu\text{m}$, and $15\ \mu\text{m}$ were resolved with 70%, 55%, and 30% contrast, respectively. Thus, it can be inferred that axial gap widths less than $30\ \mu\text{m}$ can be resolved, albeit with less contrast. Our previous studies showed that with a 15-MHz transducer, a $30\text{-}\mu\text{m}$ axial gap can be resolved with about 20% contrast at an axial range of 3 mm inside the chicken breast tissue.

3.2 Image Contrast and Modulation Depth at Different Ultrasound Frequencies

In this section, we study the effect of ultrasound frequency on image contrast and modulation depth. The images presented in the Fig. 3, using all four transducers, were acquired from slightly different imaging depths. We used an optically scattering sample (prepared from agar and Intralipid) with a 1-mm optical transport mean free path and with a 2.0-mm radius of curvature in the cylindrical geometry. We placed three optically absorbing objects (prepared using a $100\text{-}\mu\text{m}$ -thick latex object that was $70\text{-}\mu\text{m}$ wide along the ultrasound propagation direction), as shown in Fig. 6(a), in the center of the curvature of the prepared sample, i.e., 2.0 mm below the surface of the sample. These objects are prepared using a $100\text{-}\mu\text{m}$ -thick latex sheet, each being $70\ \mu\text{m}$ wide along the x axis, $100\ \mu\text{m}$ thick along the y axis, and 1.5 mm long along the z axis. The wide side of the object was parallel to the ultrasound beam and perpendicular to the light beam, i.e., all three objects were axially separated from each other by about $100\ \mu\text{m}$ inside the sample. Thus, the total width of the object shown in the Fig. 6(a) was about 0.5 mm

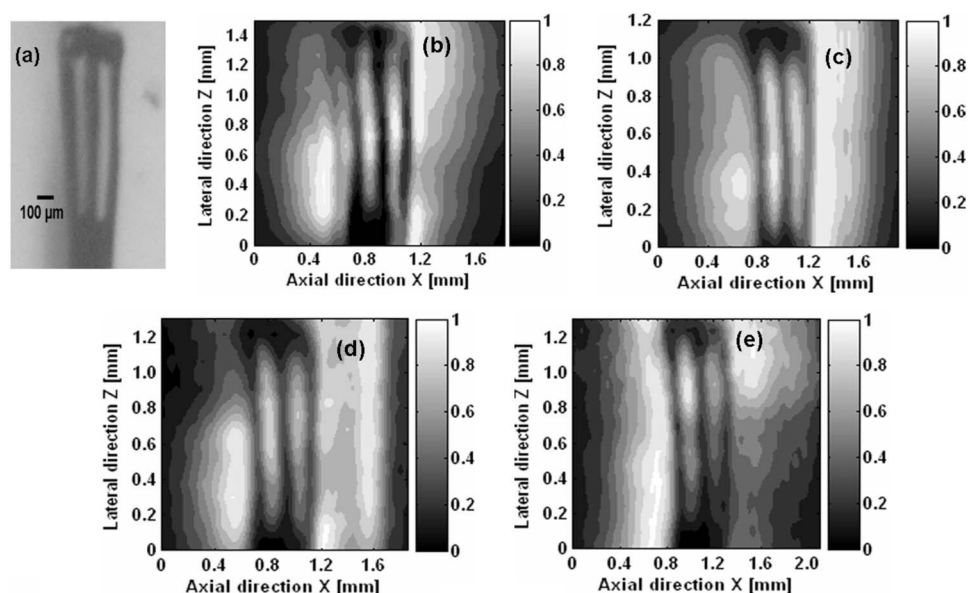


Fig. 6 Imaging of three optically absorbing objects located 2.0 mm inside the tissue-mimicking phantom along the ultrasound propagation direction, with all four high-frequency ultrasound transducers. (a) Photograph of three optically absorbing objects. B-scan UOT images of (a) obtained with (b) 15-MHz transducer, (c) 30-MHz transducer, (d) 50-MHz transducer, and (e) 75-MHz transducer.

in the axial direction, which is greater than or equal to the focal zone of all four transducers.

Figures 6(b)–6(e) present the UOT images of the object in Fig. 6(a), obtained with the four ultrasonic transducers. As in the preceding section, these 2-D images were obtained by scanning the sample along the z direction and acquiring the 1-D image that represents normalized profiles of the modulated light intensity along the x axis. These images show an axial depth range of about 2 mm for all transducers. In all these images, we notice that all three objects are axially well resolved (the top surface and the bottom surface of all three absorbing objects are clearly seen) without any significant blurring. Although all four transducers produce images of good resolution and high optical contrast, the best contrast was obtained using the 30-MHz transducer.

The modulation depth (MD), defined as the ratio of ultrasound-modulated optical intensity to the unmodulated light intensity, decreases with an increase in ultrasound frequency, because the attenuation of ultrasound pulse energy increases with an increase in the frequency when the pressure is held constant. To further understand the effect of the ultrasound (modulation) frequency on the MD, we carried out experiments with all four transducers using chicken breast samples. First we focused all four transducers about 2 mm (along the x axis) below the surface of the chicken breast sample and moved toward the surface in steps of $50 \mu\text{m}$. At each step, we calculated the MD. Figure 7(a) presents the value of the modulation depth (MD) as a function of the distance of the ultrasound focus from the surface of the chicken breast tissue sample. For all four transducers, the value of MD was highest ($\sim 1\%$) at the surface of the sample ($\sim 100 \mu\text{m}$), where the focused beams of light and ultrasound interact as if in an optically clear medium. With increased distance of the ultrasound focal point from the sample surface, the value of the MD decreases. A more rapid decay rate of the MD is

observable at higher ultrasound frequencies and close to the sample surface in the region where the light is not completely diffused. Besides ultrasound modulation frequency, the MD in general depends also on both the optical¹³ and mechanical properties¹⁴ of the sample, as well as on the optical and ultrasonic source parameters.

The trend observed in Fig. 7(a) can be explained analytically. Sakadzic and Wang¹² discussed in detail the effect of ultrasound frequency on the three different mechanisms of ultrasound modulation of light in an optically turbid medium, which are represented by the optical phase accumulation terms $C_{n,\bar{s}}$, $C_{d,\bar{s}}$, and $C_{nd,\bar{s}}$. Here, $C_{n,\bar{s}}$ and $C_{d,\bar{s}}$ represent contributions due to the modulated optical index of refraction and the modulated displacement of optical scatterers. Whereas $C_{nd,\bar{s}}$ represents the anticorrelation between the two mechanisms of modulation (and is negative), \bar{s} represents the average path length s within the ultrasound field. Later Zemp et al.²⁸ derived an analytical expression for MD in terms of these three phase accumulation terms. For moderate ultrasound pressures and in the weak scattering approximation, the modulation depth is expressed as $MD \approx (1/2)(C_{n,\bar{s}} + C_{d,\bar{s}} + C_{nd,\bar{s}})$. With reference to these studies, we plot in Fig. 7(b) the MD as a function of the average number of scattering events denoted as s/l for all four ultrasound frequencies. We choose the kinematic viscosity of water $k=10^{-6} \text{ m}^2 \text{ s}^{-1}$, the elasto-optic coefficient of water $\eta=0.32$, and $\Lambda = 2n_0k_0P_0/\rho v_a = 1 \text{ m}^{-1}$. Also it is assumed that scatterers follow the fluid displacement, i.e., $S=1$ and $\phi=0$; $k_0=2\pi/\lambda_0$ is the magnitude of the optical wave vector; v_a is the velocity of sound in water $1.5 \text{ mm}/\mu\text{s}$; and ρ is the mass density.

As shown in Fig. 7(b), the MD decreases with an increase in the ultrasound frequency. According to Sakadzic and Wang,¹² this trend can be explained as follows: In the low ultrasound frequency range, all of the scatterers are within a

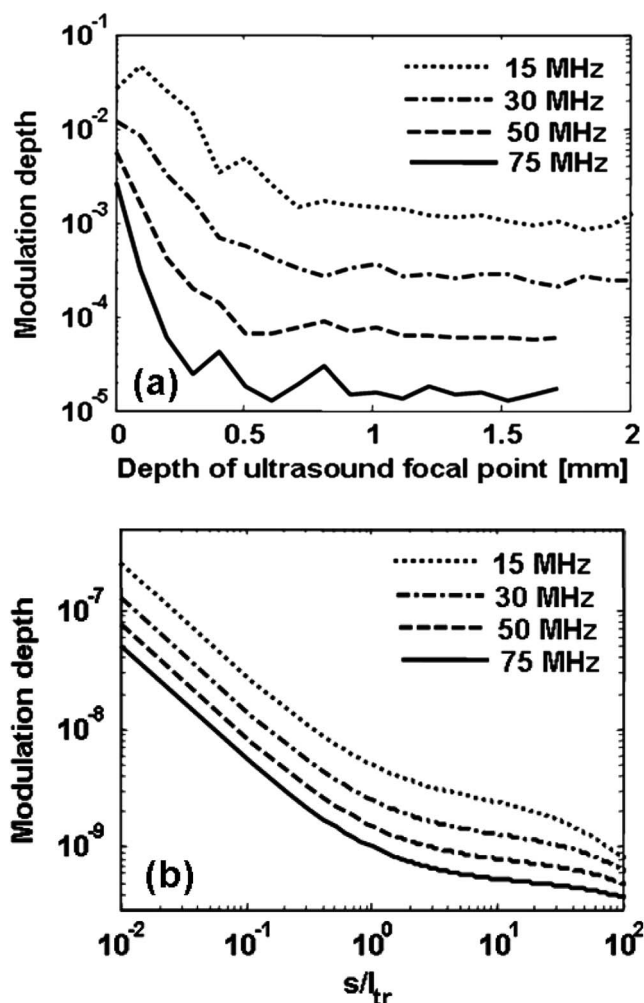


Fig. 7 (a) Experimental measurement of modulation depth as a function of the ultrasound focal point location inside the chicken breast tissue for all four high-frequency ultrasound transducers. (b) Numerical simulation of modulation depth as a function of the average number of scattering events s/l , for ultrasound frequencies of 75 MHz, 50 MHz, 30 MHz, and 15 MHz.

space with almost the same phase of the ultrasound field. This increases correlation among the phase increments associated with different scattering events along the optical path. Thus, the contribution due to the refractive index term C_n adds constructively to the total sum of C -terms. Depending on the average number of scattering events, s/l , the MD can be inversely proportional to the square of the ultrasound frequency. However, at high ultrasound frequencies, there is an increased cancellation of the phase increments in the summation of C -terms, and an inverse linear dependence of modulation depth on ultrasound frequency is observed. This dependence is due to the displacement term $C_{d,\bar{s}}$. At higher ultrasound frequencies when the pressure amplitude is kept constant, $C_{d,\bar{s}}$ is proportional to the square of the amplitude of the scatterer displacement, i.e., inversely proportional to the square of the ultrasound frequency.

4 Conclusions

In summary, this study demonstrated the feasibility of using a high ultrasound frequency transducer with a central frequency

of 75 MHz to obtain microscale resolution and high-contrast images with ultrasound-modulated optical tomography in biological tissues at an imaging depth of about 2 mm. We also obtained B-scan images using other high-frequency transducers with central frequencies of 15 MHz, 30 MHz, and 50 MHz and compared the performance of these transducers. The axial and lateral resolutions were improved from 70 μm and 140 μm (with the 15-MHz transducer) to about 30 μm and 38 μm (with the 75-MHz transducer). The axial resolutions obtained with all four transducers were better than respective lateral resolutions. Our study shows that image contrast and modulation depth decreases with an increase in ultrasound modulation frequency at any imaging depth. This technology has the potential to complement other imaging modalities that provide micron-scale resolution at a few mm imaging depths.

Acknowledgments

We thank Dr. S. Sakadzic for fruitful scientific and technical discussions and Dr. K. Maslov for preparing acoustic lenses for all four transducers used in our experiments. This research was supported by the National Institutes of Health through Grant Nos. R33 CA094267 and R01 CA106728.

References

1. T. F. Massoud and S. S. Gambhir, "Molecular imaging in living subjects: seeing fundamental biological processes in a new light," *Genes Dev.* **17**, 545–580 (2003).
2. R. Weissleder and V. Ntziachristos, "Shedding light onto live molecular targets," *Nat. Med.* **9**, 123–128 (2003).
3. H. F. Zhang, K. Maslov, G. Stoica, and L.-H. Wang, "Functional photoacoustic microscopy for high-resolution and noninvasive *in vivo* imaging," *Nat. Biotechnol.* **24**, 848–851 (2006).
4. J. G. Fujimoto, "Optical coherence tomography for ultrahigh resolution *in vivo* imaging," *Nat. Biotechnol.* **21**, 1361–1367 (2003).
5. H. Inoue, S. Kudo, and A. Shiokawa, "Laser-scanning confocal microscopy and endocytosis for cellular observation of the gastrointestinal tract," *Nat. Clin. Pract. Gastroenterol. Hepatol.* **2**, 31–37 (2005).
6. F. A. Marks, H. W. Tomlinson, and G. W. Brooksby, "A comprehensive approach to breast cancer detection using light: photon localization by ultrasound modulation and tissue characterization by spectral discrimination," *Proc. SPIE* **1888**, 500–510 (1993).
7. L. V. Wang, S. L. Jacques, and X. Zhao, "Continuous-wave ultrasonic modulation of scattered laser light to image objects in turbid media," *Opt. Lett.* **20**, 629–631 (1995).
8. W. Leutz and G. Maret, "Ultrasonic modulation of multiply scattered light," *Physica B* **204**, 14–19 (1995).
9. M. Kempe, M. Larionov, D. Zaslavsky, and A. Z. Genack, "Acousto-optic tomography with multiply scattered light," *J. Opt. Soc. Am. A* **14**, 1151–1158 (1997).
10. L. V. Wang, "Mechanisms of ultrasonic modulation of multiply scattered coherent light: an analytic model," *Phys. Rev. Lett.* **87**, 043903 (2001).
11. S. Sakadzic and L. V. Wang, "Ultrasonic modulation of multiply scattered coherent light: an analytical model for anisotropically scattering media," *Phys. Rev. E* **66**, 026603 (2002).
12. S. Sakadzic and L. V. Wang, "Modulation of multiply scattered coherent light by ultrasonic pulses: analytical model," *Phys. Rev. E* **72**, 036620 (2005).
13. S.-R. Kothapalli, S. Sakadzic, C. Kim, and L. V. Wang, "Imaging optically scattering objects with ultrasound-modulated optical tomography," *Opt. Lett.* **32**, 2351–2353 (2007).
14. X. Xu, H. Zhang, D. Qing, C. Kim, P. Hemmer, and L. V. Wang, "Photorefractive detection of tissue optical and mechanical properties by ultrasound modulated optical tomography," *Opt. Lett.* **32**, 656–658 (2007).
15. L. V. Wang and G. Ku, "Frequency-swept ultrasound-modulated optical tomography of scattering media," *Opt. Lett.* **23**, 975–977 (1998).

16. S. Leveque, A. C. Boccara, M. Lebec, and H. Saint-Jalmes, "Ultrasonic tagging of photon paths in scattering media: parallel speckle modulation processing," *Opt. Lett.* **24**, 181–183 (1999).
17. G. Yao, S.-L. Jiao, and L. V. Wang, "Frequency-swept ultrasound-modulated optical tomography in biological tissue by use of parallel detection," *Opt. Lett.* **25**, 734–736 (2000).
18. A. Lev, Z. Kotler, and B. G. Sfez, "Ultrasound tagged light imaging in turbid media in a reflectance geometry," *Opt. Lett.* **25**, 378–380 (2000).
19. M. Hisaka, T. Sugiura, and S. Kawata, "Optical cross-sectional imaging with pulse ultrasound wave assistance," *J. Opt. Soc. Am. A* **18**, 1531–1534 (2001).
20. J. Li, G. Ku, and L. V. Wang, "Ultrasound-modulated optical tomography of biological tissue by use of contrast of laser speckles," *Appl. Opt.* **41**, 6030–6035 (2002).
21. A. Lev and B. G. Sfez, "Pulsed ultrasound-modulated light tomography," *Opt. Lett.* **28**, 1549–1551 (2003).
22. M. Gross, P. Goy, and M. Al-Koussa, "Shot-noise detection of ultrasound-tagged photons in ultrasound modulated optical imaging," *Opt. Lett.* **28**, 2482–2484 (2003).
23. S. Sakadzic and L. V. Wang, "High-resolution ultrasound-modulated optical tomography in biological tissues," *Opt. Lett.* **29**, 2770–2772 (2004).
24. T. W. Murray, L. Sui, G. Maguluri, R. A. Roy, A. Nieva, F. Blonigen, and C. A. DiMarzio, "Detection of ultrasound modulated photons in diffuse media using the photorefractive effect," *Opt. Lett.* **29**, 2509–2511 (2004).
25. J. Li and L. V. Wang, "Ultrasound-modulated optical computed tomography of biological tissues," *Appl. Phys. Lett.* **84**, 1597–1599 (2004).
26. S. Sakadzic, S.-R. Kothapalli, and L. V. Wang, "Toward very high resolution imaging in ultrasound-modulated optical tomography of biological tissues," *Proc. SPIE* **6086**, 303–308 (2006).
27. American Institute of Ultrasound in Medicine (AIUM), "Mammalian *in vivo* ultrasonic biological effects," <http://www.aium.org/> (1992).
28. R. Zemp, S. Sakadzic, and L.-H. V. Wang, "Stochastic explanation of speckle contrast detection in ultrasound-modulated optical tomography," *Phys. Rev. E* **73**, 061920 (1–5) (2006).